Hollow metallic waveguides integrated with terahertz quantum cascade lasers

R. Degl'Innocenti,[1,*] Y. D. Shah,[1] D. S. Jessop,[1] Y. Ren,[1] O. Mitrofanov,[2] H. E. Beere,[1] and D. A. Ritchie,[1]

[1]*Cavendish Laboratory, University of Cambridge, J. J. Thomson Avenue, Cambridge, CB3 0HE, UK*

[2]*Department of Electronic and Electrical Engineering, University College London, Torrington Place, London, WC1E 7JE, UK*

[*]*rd448@cam.ac.uk*

Abstract: We present the realization of a compact, monolithically integrated arrangement of terahertz quantum cascade lasers with hollow metallic cylindrical waveguides. By directly mounting a copper pipe to the end facet of a double metal waveguide, it was possible to significantly improve the far field emission from such a sub-wavelength plasmonic mode, while preserving the characteristic performance of the laser. Careful alignment of the quantum cascade laser and the hollow waveguide is required in order to prevent the excitation of higher order/mixed modes as predicted with a high degree of accuracy by a theoretical model. Finally, this approach proved to be a superior method of beam shaping when compared to other *in situ* arrangements, such as a silicon hyper-hemispherical lens glued to the facet, which are presented.

OCIS codes: (140.5965) Semiconductor lasers, quantum cascade; (230.7370) Waveguides; (140.3300) Laser beam shaping.

References and links

1. M., Tonouchi, "Cutting-edge terahertz technology," Nature Photon. **1**(2), 97–105 (2007).
2. B. S. Williams, S. Kumar, H. Callebaut, and Q. Hu, "Terahertz quantum-cascade laser at 100 μm using metal waveguide for mode confinement," Appl. Phys. Lett. **83**(11), 2124–2126 (2003).
3. M. I. Amanti, M. Fischer, G. Scalari, M. Beck, and J. Faist, "Low-divergence single-mode terahertz quantum cascade laser," Nature Photon. **3**(10), 586–590 (2009).
4. M. Cui, J. N. Hovenier, Y. Ren, N. Vercruyssen, J. R. Gao, T. Y. Kao, Q. Hu, and J. L. Reno, "Beam and phase distributions of a terahertz quantum cascade wire laser," Appl. Phys. Lett. **102**(11), 111113 (2013).
5. G. Xu, R. Colombelli, S. P. Khanna, A. Belarouci, X. Letartre, L. Li, E. H. Linfield, A. G. Davies, H. E. Beere, and D. A. Ritchie, "Efficient power extraction in surface-emitting semiconductor lasers using graded photonic heterostructures," Nature Commun. **3**, 952 (2012).
6. N. Yu, Q. J. Wang, M. A. Kats, J. A. Fan, S. P. Khanna, L. Li, A. G. Davies, E. H. Linfield, and F. Capasso, "Designer spoof surface plasmon structures collimate terahertz laser beams," Nature Mater. **9**(9), 730–735 (2010).
7. W. Maineult, P. Gellie, A. Andronico, P. Filloux, G. Leo, C. Sirtori, S. Barbieri, E. Peytavit, T. Akalin, J.-F. Lampin, H. E. Beere, and D. A. Ritchie, "Metal-metal terahertz quantum cascade laser with micro-transverse electromagnetic-horn antenna," Appl. Phys. Lett. **93**(18), 183508 (2008).
8. A. W. M. Lee, Q. Qin, S. Kumar, B. S. Williams, Q. Hu, and J. Reno, "High power and high temperature THz quantum-cascade lasers based on lens-coupled metal-metal waveguides," Opt. Lett. **32**(19), 2840–2842 (2007).
9. A. W. M. Lee, B. S. Williams, S. Kumar, Q. Hu, and J. Reno, "Tunable terahertz quantum cascade lasers with external gratings," Opt. Lett. **35**(7) 910–912 (2010).
10. A. A. Danylov, J. Waldman, T. M. Goyette, A. J. Gatesman, R. H. Giles, K. J. Linden, W. R. Neal, W. E. Nixon, M. C. Wanke, and J. L. Reno, "Transformation of the multimode terahertz quantum cascade laser beam into a Gaussian, using a hollow dielectric waveguide," Appl. Opt. **46**(22), 5051–5055 (2007).

#213488 - $15.00 USD Received 17 Jun 2014; revised 22 Aug 2014; accepted 25 Aug 2014; published 29 Sep 2014

11. J. A. Harrington, R. George, P. Pedersen, and E. Mueller, "Hollow polycarbonate waveguides with inner Cu coatings for delivery of terahertz radiation," Opt. Express **12**(21), 5263–5268 (2004).
12. O. Mitrofanov and J. A. Harrington, "Dielectric-lined cylindrical metallic THz waveguides: mode structure and dispersion," Opt. Express, **18**(3), 1898–1903 (2010).
13. B. Bowden, J. A. Harrington, and O. Mitrofanov, "Low-loss modes in hollow metallic terahertz waveguides with dielectric coatings," Appl. Phys. Lett. **93**(18), 181104 (2008).
14. M. S. Vitiello, J-H. Xu, M. Kumar, F. Beltram, A. Tredicucci, O. Mitrofanov, H. E. Beere, and D. A. Ritchie, "High efficiency coupling of Terahertz micro-ring quantum cascade lasers to the low-loss optical modes of hollow metallic waveguides," Opt. Express **19**(2), 1122–1130 (2011).
15. M. S. Vitiello, J-H. Xu, F. Beltram, A. Tredicucci, O. Mitrofanov, J. A. Harrington, H. E. Beere, and D. A. Ritchie, "Guiding a terahertz quantum cascade laser into a flexible silver-coated waveguide," J. Appl. Phys. **110**(6), 063112 (2011).
16. S. Barbieri, J Alton, H. E. Beere, J. Fowler, E. H. Linfield, and D. A. Ritchie, "2.9 THz quantum cascade lasers operating up to 70 K in continuous wave," Appl. Phys. Lett. **85**(10), 1674 (2004).
17. A. W. M. Lee, B. S. Williams, S. Kumar, Q. Hu, and J. Reno, "Real-time imaging using a 4.3-THz Quantum Cascade Laser and a 320×240 Microbolometer Focal-Plane Array," IEEE Photon. Technol. Lett. **18**(3), 1415–1417 (2006).
18. U. Siciliani de Cumis, J.-H. Xu, L. Masini, R. Degl'Innocenti, P. Pingue, F. Beltram, A. Tredicucci, M. S. Vitiello, P. A. Benedetti, H. E. Beere, and D. A. Ritchie, "Terahertz confocal microscopy with a quantum cascade laser source," Opt. Express **20**(20), 21924–21931 (2012).
19. R. Degl'Innocenti, M. Montinaro, J.-H. Xu, V. Piazza, P. Pingue, A. Tredicucci, F. Beltram, H. E. Beere, and D. A. Ritchie, "Differential Near-Field Scanning Optical Microscopy with THz quantum cascade laser sources," Opt. Express **17**(26), 23785–23792 (2009).

1. Introduction

Terahertz (THz) quantum cascade lasers (QCLs) represent a unique source for a variety of applications, such as biomedical research, astronomy and material inspection [1]. In many research areas a Gaussian-like, low divergent beam shape emission is required and therefore a huge effort in the QCL community has been carried out in shaping the far field beam profile. While single plasmon THz QCLs have a better emission profile, double metal (DM) QCLs [2] offer superior temperature performance but present, due to the subwavelength mode confinement, highly divergent and irregular beam shapes. Our motivation is to combine the high operating temperature of DM QCLs with a predictable Gaussian-like beam pattern, thus overcoming the optical mismatch due to the emission from a sub-wavelength, plasmonic mode. Among the many approaches currently targeting this objective, it is worth mentioning third order Bragg grating THz QCLs [3, 4], where the improved beam profile is obtained due to the coherent superposition of emission from several QCL segments, each acting as a single antenna emitter. Alternatively, a vertically emitting graded distributed feedback bragg (DFB) grating QCL, has also demonstrated an excellent far field emission pattern [5], again by introducing a periodic structure in the QCL waveguide. Spoof surface plasmon structures, that are fabricated onto the facet of a DM QCL by using focused ion beam milling [6], are alternative to surface emitting devices. However, all the above approaches introduce a frequency selective element making them unsuitable for experiments that require a broadband frequency operation range. A beam shaping non-frequency selective approach is based on electromagnetic horn antennas. They have been successfully coupled to DM QCLs to shape the beam pattern [7]. Although this approach was efficient in improving the directionality of the output beam it did not improve the beam shape, which still exhibited a number of lobes.

The most successful attempt to improve the far-field emission, in terms of output power and beam quality using an *in situ* optical element was realized by attaching a high resistivity (in order to minimize terahertz absorption and to avoid shortening of the device) silicon lens directly onto the QCL facet [8, 9]. This approach has been so far the most effective method for improving the beam shape from DM THz QCLs that also allows a broad frequency range to be supported. Therefore, it represents the standard method our results should be compared with.

#213488 - $15.00 USD Received 17 Jun 2014; revised 22 Aug 2014; accepted 25 Aug 2014; published 29 Sep 2014

Our approach implements an alternative beam shaping element in the cryostat; a hollow copper pipe waveguide. In fact, hollow dielectric [10] and metallic [11–14] waveguides (wgs) have proven to be a very efficient way of guiding THz light with extremely low attenuations and low dispersion. Furthermore, the possibility of employing flexible waveguides [15], offers new possibilities for their implementation into many applications, such as in imaging and spectrosopy. In the literature, metallic waveguides have only been reported to be coupled to QCLs outside the cryostat, thus requiring focusing optics and a precisel and continuous alignment of the set-up in order to achieve a stable arrangement. By integrating the QCL with a hollow metallic pipe waveguide *in situ*, we have realized a compact and stable arrangement, combining the desired beam profile characteristics of the hollow copper pipes with the emission properties of a DM QCL. Furthermore, the different modes that could be excited in the copper pipes have been correctly identified and theoretically simulated, in good agreement with the experimental results. Finally, in order to obtain a direct comparison with the benchmark approach for improving the DM QCL outcoupling, a set of measurements with a similar QCL incorporating a Si hyper-hemispherical lens directly attached to the facet was performed and the output beam profile recorded and analyzed.

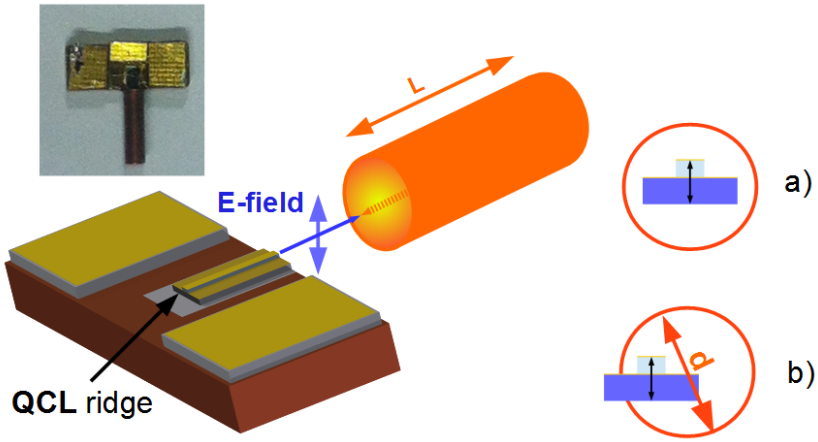

Fig. 1. Schematic of the DM QCL coupled to a hollow metallic waveguide with a length L of 11 mm and a inner diameter d of 1.7 mm. The relative positioning between the QCL and the waveguide is critical: alignment of the QCL with the waveguide axis (a) results in efficient excitation of the dominant mode, whereas misalignment (b) can lead to the excitation of the higher order modes.

2. Fabrication

A bound to continuum active region design QCL [16], with a centre frequency emitting at around 2.85 THz, was selected for this experiment. After standard Au-Au thermocompressive wafer-bonding, the AR region material was processed into ridge waveguides by photolithography and wet etching, followed by Ti /Au (10/200 nm) metal deposition for the realization of the top contact. The final ridges have a width of 120 μm, a height of 12.5 μm and a length between 1 and 2 mm. The QCLs were then cleaved and mounted to copper blocks and wire bonded to ceramic pads. A set of identical, except for the length, QCLs were realized out of the same wafer, in order to ensure consistency between the different measurements. The hollow copper waveguides attached to the DM QCLs have a typical length of 7-11 mm, and an inner diameter of 1.7 mm. Since these waveguides also support higher order modes with losses negligible over

#213488 - $15.00 USD Received 17 Jun 2014; revised 22 Aug 2014; accepted 25 Aug 2014; published 29 Sep 2014

these lengths (transmission loss for TE_{11} <0.05 dB over these distances in Cu wgs with similar diameters [11]), consequently, the alignment between the QCLs and the copper pipes represents the most critical step that has to be undertaken carefully. In fact, a small relative misalignment can lead to the excitation of higher order or mixed modes, yielding an output that would not be usable in many QCL applications [17–19], or could not be efficiently matched to a similar external waveguide. The critical alignment between the QCLs and the hollow waveguides has been carried out by using micrometer translators for both the wgs and the QCLs and an optical microscope for monitoring the relative distance. We estimate that a precision of $\simeq$10-20 μm was achieved. A UV sensitive adhesive (Loctite 358) was used for attaching the waveguide. The hollow waveguide was placed in contact with the copper mount, a few microns from the laser facet. The final arrangement of the QCL and copper pipe, presented in Fig.1 is robust and could stand several thermal cycles at cryogenic temperatures. Depending on the relative position between the hollow waveguide and the laser facet, we distinguished and analyzed the two extreme cases presented in Figs. 1(a) and 1(b), where the out of axis alignment has been exaggerated (the misalignment between the two objects presented in Fig. 1(b) was estimated to be around 300 μm). The purpose for this extreme comparison is because we wanted to quantify from an experimental point of view how critical the alignment is. However, optimum alignment allows us to achieve similar results in more than one QCL, thus validating the reproducibility of this method. The QCL + wg arrangement is then mounted onto a copper cold finger and characterized at cryogenic temperatures.

3. Experiments: power and temperature characterization

In order to quantify the impact of the hollow waveguide on the performances of the QCL, we performed a set of measurements with and without the waveguide. The voltage-current (VI) and light-current (LI) characteristics are shown in Fig. 2(a) for the QCL without waveguides, and in the arrangement of Figs. 1(a) and 1(b). The implementation of an 11 mm long copper pipe does not affect the light-current-voltage (L-I-V) curves, which exhibit values and trends similar to the characteristic curves of the QCL without waveguides. In particular, the VI curves for the arrangements of QCL/copper pipe described in Figs. 1(a) and 1(b) are almost identical. The output power from the 11 mm from the QCL with the wg was recorded with a Golay cell and a lock-in amplifier. Fig. 2(a) shows that in the configuration depicted in Fig. 1(a) the output power measured is reduced to $\simeq$ 50 % of the total power measured without the wg, and even lower in the out of axis alignment; this is expected since the coupling of the emitted light into a higher order mode is less efficient. The power drop after the addition of the waveguide is a consequence of the efficiency of the coupling to the mode excited in the copper pipe of the light emitted from the QCL facet, which is otherwise reflected or scattered. Another critical factor which is analysed in our approach is the temperature performance of a QCL coupled with the copper wg. The assumption of a marginal impact of those wgs on the effective temperature of the metal cold finger is not trivial. Fig. 2(b), reports the threshold current densities J_{TH} at different temperatures for the same QCL with and without wg. The introduction of the hollow pipe *in situ* did not significantly alter the maximum operation temperature T_{Max}. The small discrepancy, T_{Max} = 75 K with the hollow waveguide attached and T_{Max} = 82 K without, can be also attributed to an imperfect contact between the laser and the cold finger. In order to get further insight into the temperature characteristics of the QCL+ wg arrangement, the two sets of data presented in Fig. 2(b) were fitted using the usual formula $J_{TH} = J_{TH0} + A \cdot exp^{T/T_0}$ where J_{TH0}, A, and T_0 were left as free fitting parameters. The curves that best fit the experimental data are reported in Fig. 2(b), and yield the values for J_{TH0} and T_0 of 165$\pm$4 Acm^{-2} and 15$\pm$1 K for the QCL without waveguide, and 141$\pm$5 Acm^{-2} and 21$\pm$1 K for the QCL with the waveguide. The increase in the current threshold J_{TH} observed after the addition of the wg in both the two

#213488 - $15.00 USD Received 17 Jun 2014; revised 22 Aug 2014; accepted 25 Aug 2014; published 29 Sep 2014

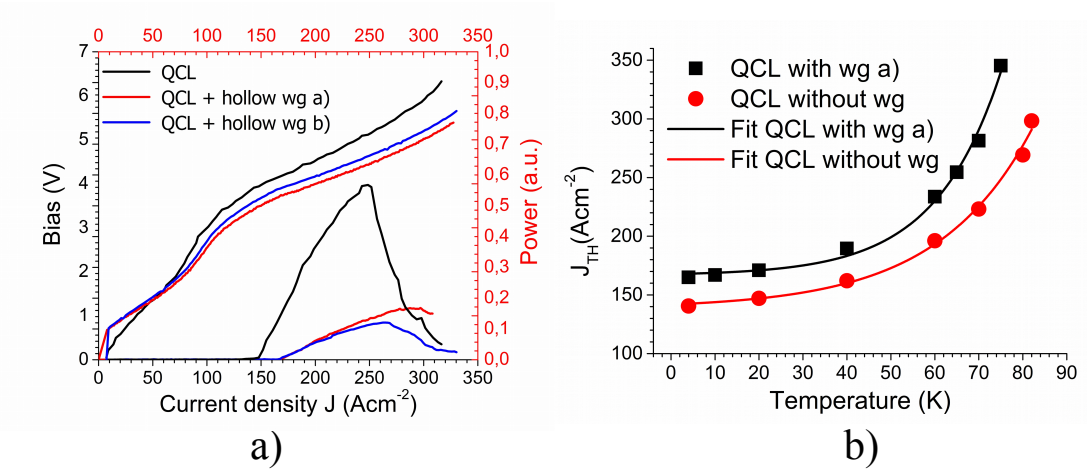

Fig. 2. a) Voltage-current and light-current curves of a 2.9 mm, 120 μm wide ridge QCL in the three different configuration, without the waveguide and in the arrangements of Figs. 1(a) and 1(b). The laser was biased in pulsed operation at 100 kHz and with 10% duty cycle at 4 K temperature. b) A comparison between the threshold current density J_{TH} of the same QCL, with and without the copper waveguide attached in the configuration of Fig. 1(a). The solid lines represent the best fit to the experimental data

arrangements of Figs. 1(a) and 1(b) is attributed to the different effective temperature of the QCL because of the copper pipe. The difference in the parameter T_0, which is a measure of the temperature performance of a QCL, of $\simeq$ 6 K is in good agreement with the discrepancy of $\simeq$ 7 K registered between the maximal operational temperatures of the QCL in the two configurations.

4. Critical coupling

In order to acquire the beam profile a Golay cell was positioned onto a computer controlled, motorized XYZ translation stage with a minimum step-size of 0.15 mm in x and y directions. An intensity map was recorded at different distances z between the end of the hollow waveguide and the detector. An aperture with a diameter of $\simeq$ 1.5 mm, was placed in front of the Golay Cell during all the far-field measurements. The QCL was operated in the same experimental conditions (same bias applied to the laser, a pulse repetition rate of 100 kHz, a duty cycle of 15% and a cold finger temperature of 4 K).

The two situations reported in Figs. 1(a) and 1(b) yield completely different beam patterns, as it is shown in Fig. 3. The experimental emission distribution in Fig. 3(a) exhibits a slight ellipticity, with the minor axis of the ellipse along the direction of the polarization. The experimental profile is similar to the far-field pattern of the TE_{11} mode of the cylindrical metallic waveguide. For comparison, Fig. 3(a) also shows the TE_{11} mode pattern calculated using the diffraction integral and the classical analytical model for the TE_{11} mode. Conversely, in the case of an extreme misalignment between the QCL facet and hollow pipe, as illustrated in Fig. 1(b), the far-field pattern acquired has a characteristic three lobe shape in Fig. 3(b). The experimental pattern cannot be matched to any single mode supported by the cylindrical metallic waveguide. However a superposition of the TE_{01} and TM_{31} modes can produce an intensity pattern with the 3-fold symmetry. The calculated pattern in Fig. 3(b) shows a good agreement with the measured profile. Details of the calculations are discussed in Appendix A. Therefore, careful alignment

#213488 - $15.00 USD Received 17 Jun 2014; revised 22 Aug 2014; accepted 25 Aug 2014; published 29 Sep 2014

of the hollow copper wg axis with the QCL results in the excitation of the lowest order mode, with a Gaussian-like far-field profile. The beam profile of the DM quantum cascade laser before the addition of the hollow metal waveguide is reported in Fig. 3(c) for completeness. As it can be observed, although the total power registered without the wg is higher than the output power measured in the configuration of Fig. 1(a), this result is achieved by integrating the contributions of different lobes, which limits the practical use of such emitted light. Since the light is directly diverging from a subwavelength aperture, the pattern is also more diffracted with respect to the configurations of Figs. 1(a) and 1(b), even though the multi-lobe irregular emission and the relatively short distance between laser and detector, do not allow to fully appreciate the beam ellipticity. Furthermore, it is possible to notice in Fig. 3(c) interference fringes arising from the reflection from the back facet of the laser to the ceramic pad also shown in Fig. 1. While such an interference pattern could be avoided by placing a suitable absorber between the back facet and the cryostat window/ceramic pad, it is worth pointing out that the our approach also helped in removing this undesirable effect.

5. Comparison between high resistivity Si lens and hollow copper waveguide

In the literature there has been reported a number of diverse experiments aiming to improve the beam quality from DM THz QCLs. One of the most successful approaches consists in a high resistivity silicon lens directly attached to a QCL facet. The higher power and improved emission observed were mostly attributed to the increased collection efficiency and to a reduced optical mismatch between the mode in the waveguide and the mode propagating outside. A silicon spacer was also added to the hemispherical lens in order to obtain a more collimated output beam, as in [9]. In order to perform a direct comparisons between these two approaches an experiment similar to [8] was reproduced. A high resistivity hyper-hemispherical Si lens with a diameter of 3 mm and a spacer of 0.6 mm was carefully positioned onto the facet of a QCL fabricated from the same batch as was used for the copper pipes. The arrangement is schematically presented in Fig 4. The bullet-like Si lens was attached, after careful alignment, by using the same UV sensitive adhesive (Loctite 358). The thickness of the spacer was chosen in order to obtained a beam as collimated as possible. Therefore its thickness was larger than the one corresponding to the aplanatic point R/n_{Si} (where R is the hemispherical lens radius and n_{Si} is the refractive index of silicon $\simeq 3.4$), and at the same time calculated to minimize the spherical aberration. The value of the spacer of 0.6 mm for a laser having center frequency around 2.85 THz, is consistent with the 0.46 mm thicker spacer used in [8] by Lee et al. at 4.1 THz. The voltage-current characteristics are marginally affected by the addition of the Si lens while the emitted power increased, in agreement with what is reported in [8]. Our attention was mainly focused on the analysis of far-field patterns. The beam profile was acquired at different distances z between the detector, a Golay cell, and the laser, with the same procedure already mentioned for the hollow waveguides. The results are presented in Figs. 4(a), 4(b) and 4(c) corresponding to different distances from the end of the waveguide to the detector z_1 = 11 mm, z_2 = 22 mm and z_3 = 33 mm, respectively. The far-field profiles are elliptical but represent a clear improvement with respect to the emission pattern normally expected from a DM QCL, such as the one presented in Fig. 3(c). In order to investigate and quantify into more details the effective collimation achieved by the Si lens, several profiles were selected from each beam-pattern. Each profile P as function of the distance $r = \sqrt{x^2 + y^2}$ was extracted and fitted by using the formula in Eq. (1) and Eq. (2) from Gaussian optics.

$$P(A, r, r_0, w_0, \lambda_0) = A \cdot exp^{\frac{-2(r-r_0)^2}{w(z)^2}} \tag{1}$$

#213488 - $15.00 USD Received 17 Jun 2014; revised 22 Aug 2014; accepted 25 Aug 2014; published 29 Sep 2014

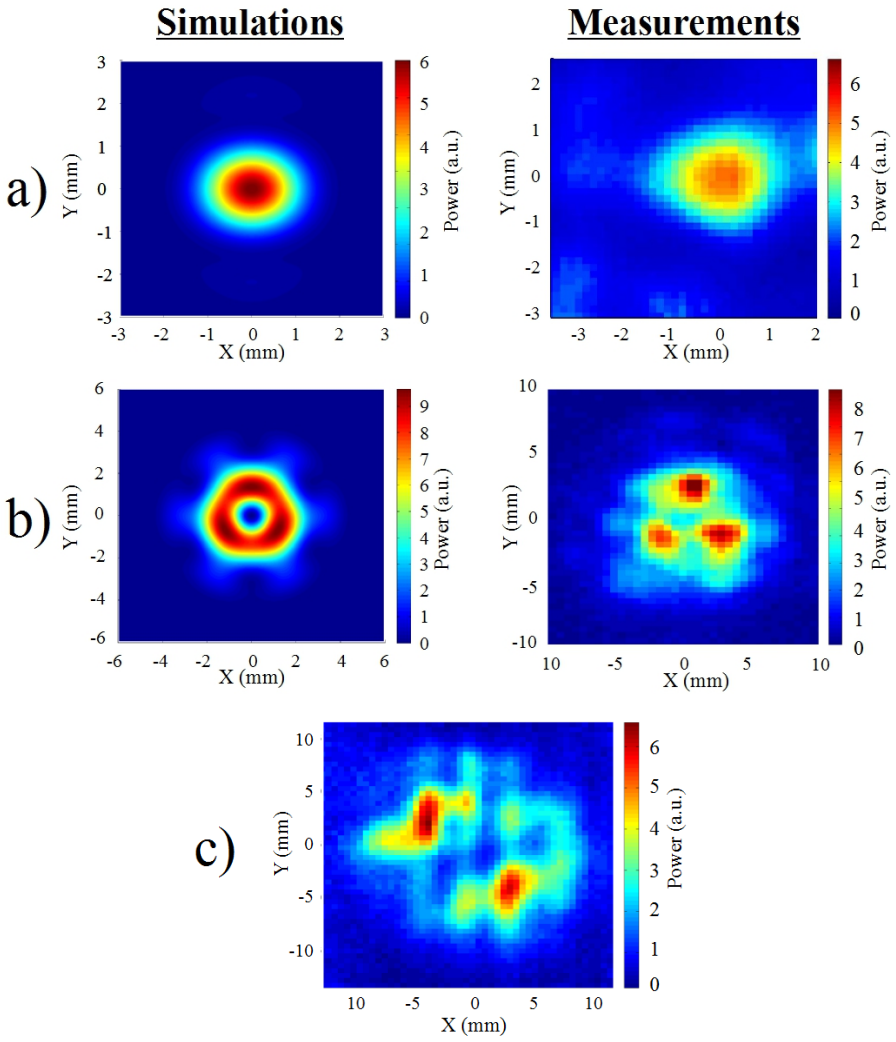

Fig. 3. Measured and theoretically predicted pattern emissions out of a 11 mm long hollow pipe at a distance z of 22 mm between the detector (Golay cell) and the waveguide aperture. All the simulations have been performed at a frequency of 2.8 THz, which is the center frequency of the QCL emission. a) The output emission from the hollow wg in the alignement configuration illustrated in Fig. 1(a); b) The beam shape in the extreme case of the out of axis alignment reported in Fig. 1(b); c) The beam profile from the QCL without the waveguide, measured at a distance z of 11 mm

#213488 - $15.00 USD Received 17 Jun 2014; revised 22 Aug 2014; accepted 25 Aug 2014; published 29 Sep 2014

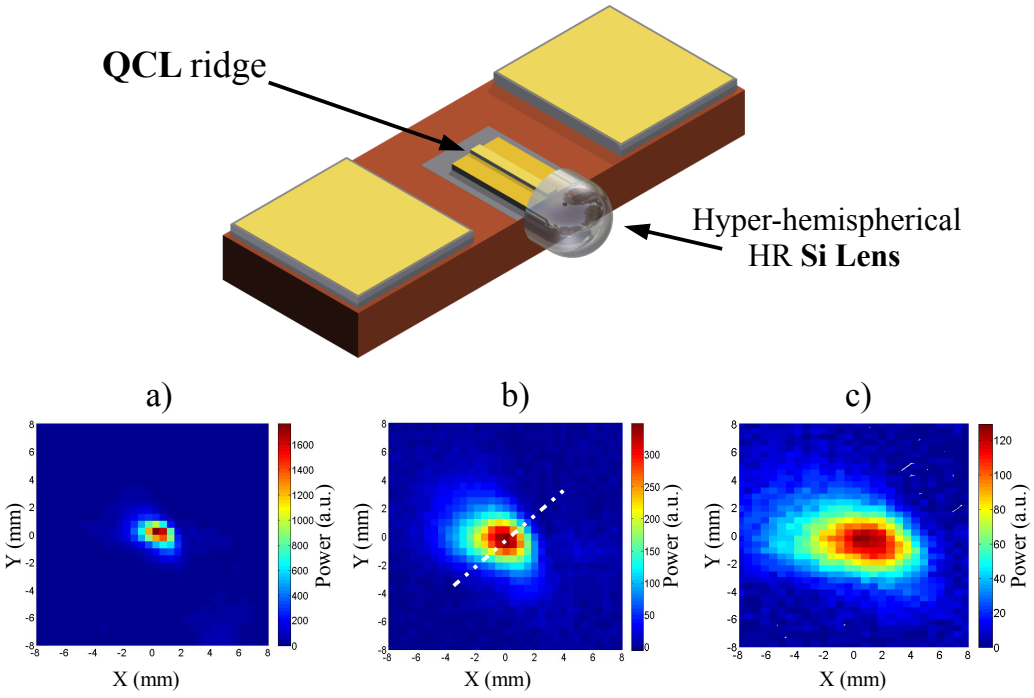

Fig. 4. Beam profiles of a QCL with a Si hyper-hemispherical lens attached to a facet (arrangement depicted in the schematic on top), corresponding to different distance z between detector and laser a) z_1 = 11 mm, b) z_2 = 22 mm, c) z_3 = 33 mm. Several profiles have been extracted for analysis and fitting along a direction similar to the one presented in b)

$$\text{where} \quad w(z) = w_0 \cdot \sqrt{1 + (z/z_0)^2} \quad \text{and} \quad z_0 = \pi w_0^2 / \lambda_0 \tag{2}$$

A and r_0 are constants while w_0 and λ_0 represent respectively the beam waist and the vacuum wavelength. The same analysis was performed for all the patterns acquired at different distances z. The values A, r_0 and w_0 were left as free fitting parameters. The results obtained from a typical fit procedure are presented in Fig. 5 while the results obtained from the three different patterns are reported in the inset. Three independent evaluations of the waist parameter w_0 were obtained from the far field patterns acquired at different distances. It should be noted that since the emission is coming from a sub-wavelength plasmonic facet coupled to an hyper-hemispherical Si lens, the definition of a waist parameter is not straightforward. In order to investigate the reproducibility of the arrangement QCL + waveguide, a second 8 mm long copper pipe was coupled to another QCL fabricated from the same batch. The analysis of the far fields, similar to the one already presented in Fig. 3(a) and acquired for completeness at three different distances z, yielded results consistent with the previous set of measurements. All the results obtained from the fitting procedure of both QCL + Si lens and QCL + hollow waveguide are presented in Table 1. The average beam waist was calculated to be 0.20 mm $\pm$ 0.03 mm for the Silicon lens coupled QCL. The profiles were extracted with an analogous procedure from the measured beam pattern corresponding to a QCL + 11 mm long copper pipe.

#213488 - $15.00 USD Received 17 Jun 2014; revised 22 Aug 2014; accepted 25 Aug 2014; published 29 Sep 2014

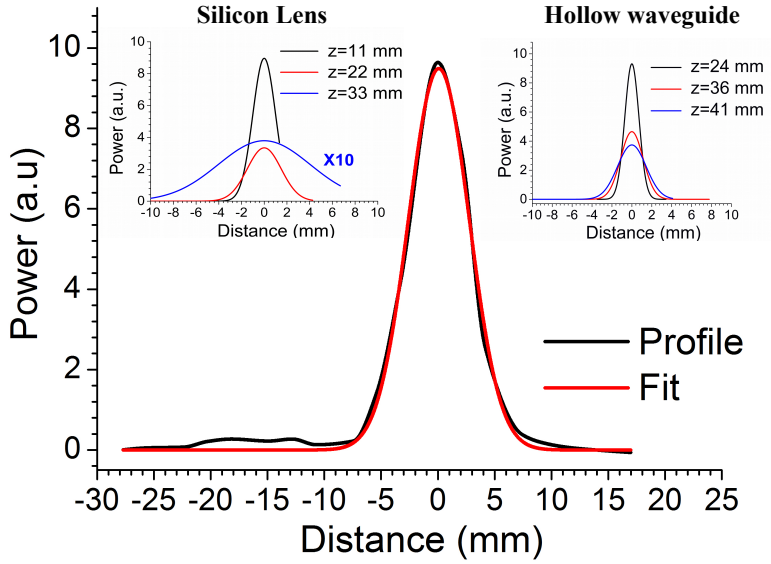

Fig. 5. Profile extracted from the beam pattern QCL + Si lens acquired at a distance of 33 mm as presented in Fig. 4(c), together with the best fit obtained by using Eq. 1. Similar fits from the other profiles are shown in the inset for both Silicon lens and Hollow waveguide coupled QCLs.

The profiles extracted from the measured far-field presented in Fig. 3(a) yielded a value for the average waist w_0 of 0.48 mm $\pm$ 0.03 mm, in good agreement with the average value of 0.50 mm $\pm$ 0.05 mm obtained from the QCL + 8 mm long waveguide. It is thus finally possible to perform a comparison between the divergence angle θ of the THz beam spot with the two approaches by using the formula from Gaussian optics for the beam divergence $\theta = \lambda_0/(\pi w_0)$. Although the introduction of a spacer increased the collimation, the THz beam out of a QCL coupled to a Silicon lens is divergent with an angle of $\simeq 10^\circ$. Conversely, the THz spot obtained with the hollow waveguide has a divergence of $\simeq 3.7^\circ$, as can be also seen in the insets in Fig. 5. This result was not unexpected since in the first case, even though the light is emitted from a dielectric medium, the Si lens, which reduces the optical mismatch between the sub-wavelength laser facet and the vacuum, it is not possible to completely overcome the plasmonic nature of the mode in the laser cavity, nor to avoid the spherical aberration. In the latter case, the light is propagating from an initial wider waist w_0 therefore reducing the diffraction and providing the ultimate beam shaping. It should be noticed that this represents a significant improvement with respect to the collimation achieved in third-order Bragg grating DFB QCLs [4].

In summary, by integrating a THz QCL with a mm-long hollow metal waveguide, the beam profile out of a DM cavity was greatly improved, without affecting the temperature characteristics of the laser. In particular, the light emission pattern is defined by a lower order mode of the hollow metallic waveguide, thus presenting a further improvement with respect to the both surface patterned, such as third order grating, and Si-lens coupled QCLs. This *in situ* approach does not require any alignment of the THz light out of the cryostat, or any complex fabrication process. The critical step of the coupling between the laser facet and the hollow waveguide, could be solved by opportunely shaping the copper block where the laser ridge is mounted, in order to aid the task of the relative alignment, and improve at the same time the laser tempera-

#213488 - $15.00 USD Received 17 Jun 2014; revised 22 Aug 2014; accepted 25 Aug 2014; published 29 Sep 2014

Table 1. Calculated values for the initial waist w_0 for the profiles extracted from the beam patterns acquired at different z values. The error is given by the reproducibility of several profiles extracted from the same far-field figure. The same procedure was applied for both cases of the QCL coupled to a Silicon lens and for the QCL coupled to an 8 mm long copper waveguide

Silicon Lens		
Distance z (mm)	w_0 (mm)	Error (mm)
11	0.21	$\pm$ 0.04
22	0.22	$\pm$ 0.03
33	0.19	$\pm$ 0.02
Copper Waveguide		
Distance z (mm)	w_0 (mm)	Error (mm)
24	0.43	$\pm$ 0.05
36	0.55	$\pm$ 0.05
41	0.52	$\pm$ 0.05

ture performance. Our approach is also competitive in terms of beam profile and collimation with a Si lens directly glued/pressed *in situ* to the laser facet. Furthermore, the coupling of hollow wgs with QCLs does not hinder the possibility to improve the laser mode matching and thus the total output power by inserting a suitable dielectric coating or optical element. Finally, our results are of particular importance in light of an efficient coupling of the mode profile in the cryostat with the mode profile of an external flexible waveguide.

6. Conclusion

We have realized the *in situ* coupling between a THz QCL and a hollow copper waveguide. This arrangement has preserved the desired characteristics of a DM QCL, while improving the beam profile. The far field patterns have been clearly identified and analyzed from both the experimental and a theoretical point of view. Finally, in order to perform a direct comparison with similar experiments for improving the beam quality *in situ*, a detailed analysis has been carried out on a QCL laser coupled to high resistivity Si lens. The results, consistent with what has already been reported in literature, confirmed the advantages of our approach in terms of beam shaping and reduced beam divergence. The beam profile obtained out of a DM QCL coupled to a copper pipe resulted to be a further improvement with respect to the beam shaping experiments reported so far.

Appendix A: Higher order mode in a hollow waveguide

Far-field beam profiles at the wg output are calculated using the classical analytical solution for the TE and TM modes in hollows metallic waveguides and the diffraction integral for a frequency of 2.8 THz over the open area of the wg. The experimental three-lobe pattern in Fig. 3(b) shows the 3-fold symmetry, which can be achieved by superimposing the TE_{01} and TM_{31} modes. The near-field intensity patterns ($|E_x^2 + E_y^2|$) calculated for each mode at $z = 0$ and at 2.8 THz are shown in Fig. 6. A superposition of $2\times TE_{01}$ and the TM_{31} mode yields a good match with the measured profile. The superposition pattern varies depending on the relative phase and amplitude of the two modes, however the 3-fold symmetry of the pattern remains.

#213488 - $15.00 USD Received 17 Jun 2014; revised 22 Aug 2014; accepted 25 Aug 2014; published 29 Sep 2014

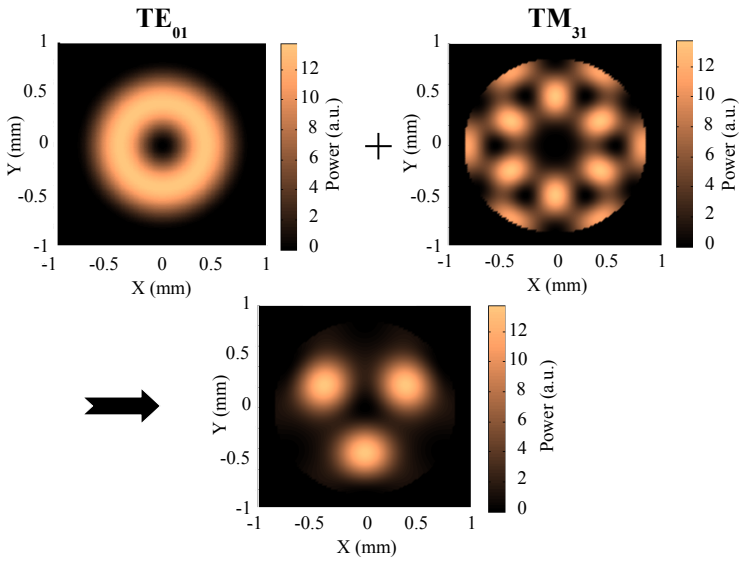

Fig. 6. Near field (z=0) pattern calculated in the configuration of Fig. 3(b). The three lobes pattern is a superposition between $2\times TE_{01}$ and one TM_{31} modes. The far field at different distances z is given by the relative intensity/phases of the two modes

Acknowledgments

The authors acknowledge financial support from the Engineering and Physical Sciences Research Council (grant number EP/J017671/1, COherent Terahertz Systems)

#213488 - $15.00 USD Received 17 Jun 2014; revised 22 Aug 2014; accepted 25 Aug 2014; published 29 Sep 2014